Supporting Information

Tsurumura et al. 10.1073/pnas.1217227110

SI Materials and Methods

Sample Preparation, Crystallization, and NAD^+ Soaking. Iota-toxin (Ia) purified from *Bacillus subtilis* contaminated small amounts of protease, which caused actin cleavage in the DNaseI-binding loop. Ia did not cause the cleavage in the βTAD (thiazole-4-carboxamide adenine dinucleotide)-Ia-actin structure reported previously; however, we used *Escherichia coli* (pET15b)-produced Ia in this report. BL21 (DE3) cells transformed with pET15b-Ia were selected on LB plates with ampicillin. A single colony was inoculated into 5 mL of LB and grown until A_{600} of ∼0.5. The culture was transferred into 1 L of LB–ampicillin and grown overnight with vigorous shaking at 37 °C. Cell were harvested by centrifugation at 4 °C at 8,000 × *g* for 5 min and resuspended in 50 mL of buffer [20 mM Tris·HCl (pH 8.0), 500 mM NaCl, 20 mM imidazole, complete EDTA-free (Roche)]. Cell were passed through a French press and centrifuged at 13,000 × *g* for 30 min. The supernatant was loaded onto Ni-NTA agarose, and the elution fraction was dialyzed against buffer A [10 mM Tris·HCl (pH 8.0)]. The sample was loaded onto a Q Sepharose column (Bio-Rad) equilibrated with buffer A and eluted using buffer A plus 1 M NaCl. The eluate was dialyzed overnight against 10 mM Tris·HCl (pH 8.0). Ia concentrated to 15 mg/mL by ultrafiltration and stored at −70 °C. Ia by *E. coli* includes five extra N-terminal residues: RGSHM.

We used newly purified Ia to make a large crystal. In addition, E378S, E380A, and E380S mutants of Ia were prepared using the same protocols. Actin preparation was described previously (1). Basically, crystallization of apo-Ia-actin and NAD^+-Ia (mutants)-actin was described before using the same protocols as prepared for βTAD-Ia-actin (1). Latrunculin A was used for the purpose of stabilizing the monomeric state of actin. To obtain large apo-Ia-actin crystals, both micro and macro seeding were applied. NAD^+ soaking of apo-Ia (WT)-actin crystals was done under two conditions. The first condition (10 mM NAD^+ soaking in cryo-protectant 30% (vol/vol) ethylene glycol for 30 min at room temperature) made NAD^+-Ia-actin. The second condition (10 mM NAD^+ soaking in crystallization mother liquor for 30 min at room temperature) made Ia-ADP ribosylated (ADPR)-actin.

Data Collection. Each crystal was picked up using a nylon loop, dipped in mother liquor supplemented with 30% ethylene glycol as a cryoprotectant, and plunged into a nitrogen-gas stream at 100 K. The crystal space group was determined to be *P*212121, and the crystal packing of Ia and actin was basically the same as in βTAD-Ia-actin. Data collection statistics, cell constants, and the final model statistics of apo-Ia-actin, NAD^+-Ia (WT and mutants)-actin, and Ia-ADPR-actin are summarized in Tables S1 and S2. Data collection was done at 100 K using an X-ray wavelength of 1.0 Å on the PF-AR NW12A and BL5A beamlines at KEK Photon Factory, using a Quantum 210r detector system. A total of 540 frames were collected with 0.3° oscillations. This strategy yielded high-resolution data sets with high quality beyond 2 Å, especially for NAD^+-Ia (WT)-actin. The diffraction images were integrated and scaled using the programs DENZO and SCALEPACK from the HKL-2000 suite (2).

Model Building, Refinement, and Comparison of the Structures. The structures of apo-Ia-actin and NAD^+-Ia (WT and mutants)-actin were determined using the molecular replacement method with MOLREP (3, 4) in CCP4i in the structure of βTAD-Ia-actin (3BUZ) in which βTAD, ATP, Latrunculin A, calcium, and waters were deleted. Each structure was refined using REFMAC5 (4) rigid body refinement because the relative positions differed. Thereafter, the model structure was refined iteratively using REFMAC5 restraint refinement and Coot (5). Finally, cofactors (NAD^+, ATP, Latrunculin A, calcium) and waters were added. Comparison of the structures was done using PyMOL (6). The structure of Ia-ADPR-actin was determined in the same manner, and the ADP-ribosylated arginine cif file was built using PRODRG (7).

Assay of ADP-Ribosylation Reaction. The crystal assay was conducted as follows: crystals of the Ia-actin complex were washed with mother liquor twice. Biotin-NAD^+ (50 μM) was the added to the mother liquor containing the Ia-actin complex, and the mixture was kept at room temperature overnight. These samples were then subjected to SDS/PAGE. The gel was washed twice with PBS, stained with streptavidin-FITC (250 nM), washed twice with PBS again, and scanned using a Typhoon FLA 9000 (General Electric). The solution assay was conducted as follows: Ia (1.6 μM) and actin (8 μM) were mixed together in mother liquor. Biotin-NAD^+ (10 μM) was then added to the mixture, which was kept at room temperature overnight. Thereafter, the same protocol used for the crystal assay was applied.

Assay of NADase Activity Using FPLC. Samples were prepared with 500 μM NAD^+ added to 10 μM (final concentration) Ia and incubated at 37 °C for 1 h. We carried out NADase activity assay by FPLC-equipped TSK-GEL column (Tosoh) with running buffer containing 100 volumes of 20 mM phosphate buffer (pH 5.5) and 5 volumes of acetonitrile at room temperature. The authentic ligands, such as NAD^+, ADP ribose, and nicotinamide, were analyzed alone with 1 mL/min flow rate. Mixtures of enzyme and NAD^+ were analyzed in the same condition.

1. Tsuge H, et al. (2008) Structural basis of actin recognition and arginine ADP-ribosylation by Clostridium perfringens iota-toxin. *Proc Natl Acad Sci USA* 105(21): 7399–7404.
2. Otwinowski Z, Minor W (1997) *Processing of X-Ray Diffraction Data Collected in Oscillation Mode* (Academic Press, New York).
3. Vagin A, Teplyakov A (2000) An approach to multi-copy search in molecular replacement. *Acta Crystallogr D Biol Crystallogr* 56(Pt 12):1622–1624.
4. Murshudov GN, Vagin AA, Dodson EJ (1997) Refinement of macromolecular structures by the maximum-likelihood method. *Acta Crystallogr D Biol Crystallogr* 53(Pt 3):240–255.
5. Emsley P, Cowtan K (2004) Coot: Model-building tools for molecular graphics. *Acta Crystallogr D Biol Crystallogr* 60(Pt 12 Pt 1):2126–2132.
6. DeLano WL (2002) *The PyMOL User's Manual* (DeLano Scientific, San Carlos, CA).
7. Debreczeni JE, Emsley P (2012) Handling ligands with Coot. *Acta Crystallogr D Biol Crystallogr* 68(Pt 4):425–430.

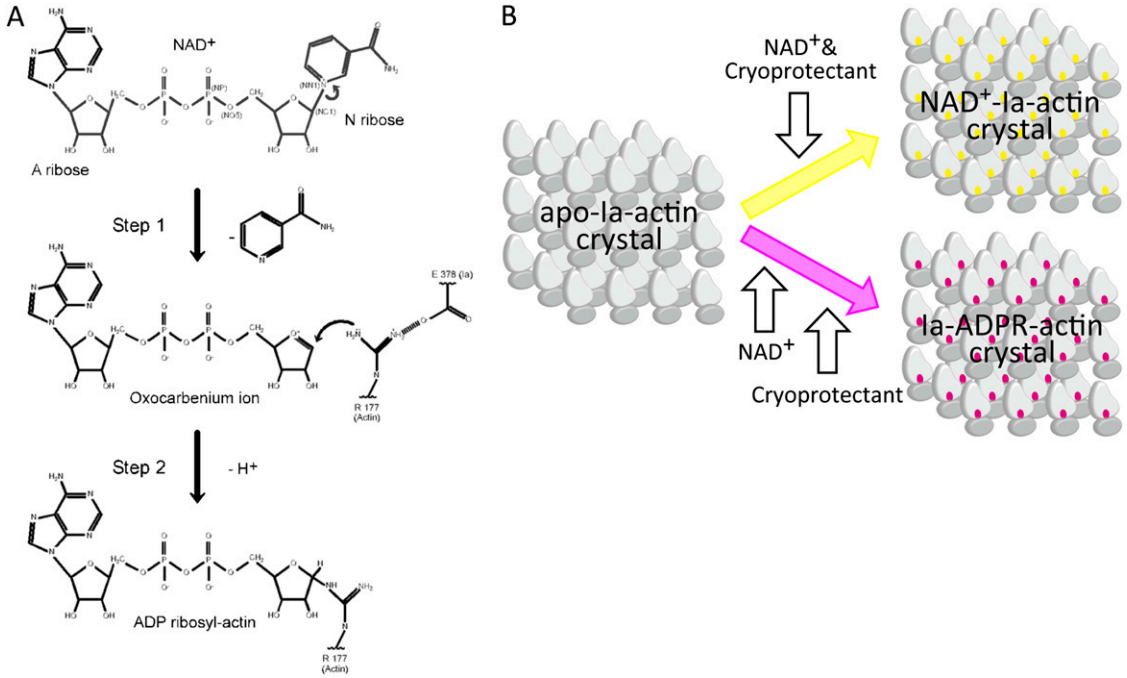

Fig. S1. (*A*) Catalytic mechanism of ADP-ribosylation reaction. Step 1: Cleavage of nicotinamide moiety and production of oxocarbenium cation. Step 2: deprotonation of Arg177 of actin and making bond between NC1 of *N*-ribose and guanidyl nitrogen of Arg177. (*B*) Protocols for soaking apo-Ia-actin crystals with NAD^+ to produce NAD^+-Ia-actin and Ia-ADPR-actin. Crystals were soaked with 10 mM NAD^+ in cryoprotectant (30% ethylene glycol) to produce NAD^+-Ia-actin. On the other hand, crystals were soaked with 10 mM NAD^+ for 30 min in mother liquor to produce Ia-ADPR-actin.

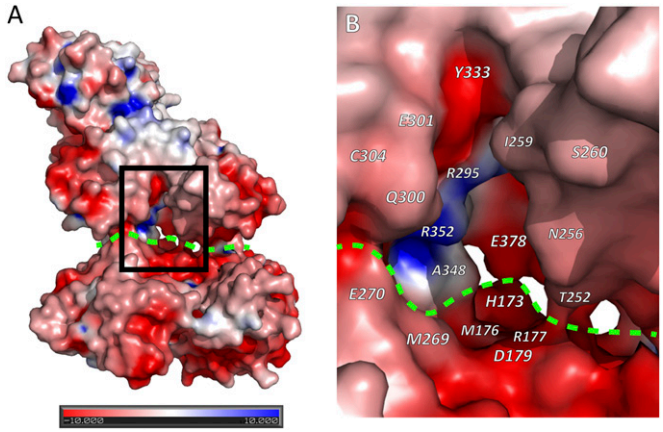

Fig. S2. (*A*) The electrostatic molecular surface of the whole structure of apo-Ia-actin. Black square is the area in *B*. (*B*) Close-up view of active site of Ia in apo-Ia-actin. Dashed bright green line is the surface between Ia and actin.

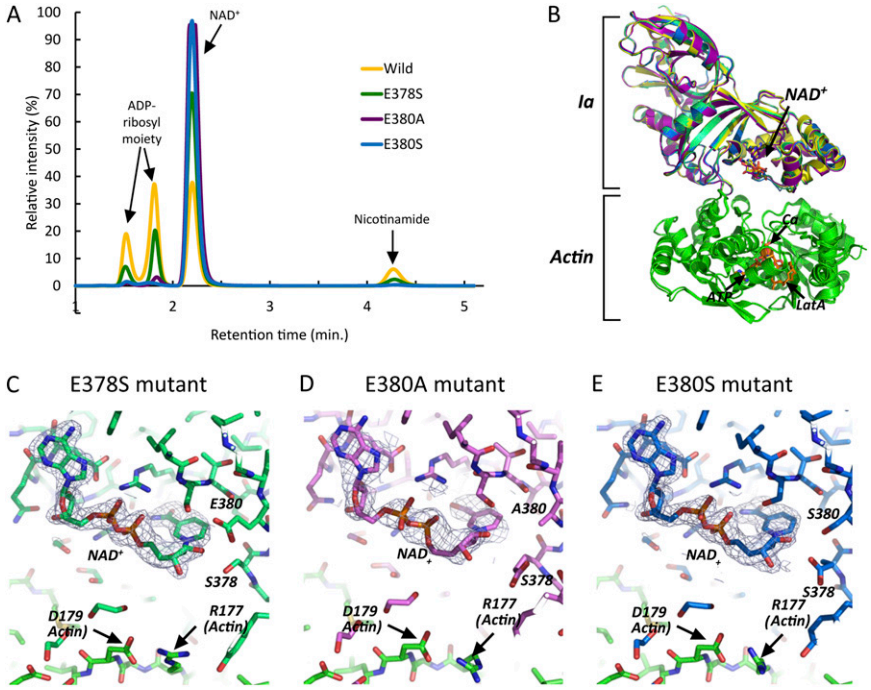

Fig. S3. (*A*) NADase activities of Ia wild type and mutants measured by FPLC. Wild type (yellow), E378S (green), E380A (purple), and E380S (blue) are illustrated. The authentic ligands were analyzed alone, resulting in two peaks of 1.5 and 1.8 min for ADP ribosyl moiety; 2.2-min peak is NAD^+, and 4.3-min peak is nicotinamide. (*B*) Overall structures of four complexes of Ia in NAD^+-Ia (WT)-actin, NAD^+-Ia (E378S)-actin, NAD^+-Ia (E380A)-actin, and NAD^+-Ia (E380S)-actin. All of the complexes show NAD^+ bound in the prereaction state. (*C*) Electron density around NAD^+ within the NAD^+-Ia (E378S)-actin, (*D*) NAD^+-Ia (E380A)-actin, and (*E*) NAD^+-Ia (E380S)-actin. All 2Fo-Fc electron density maps are at 1.0 σ. All colors are the same as in Fig. 6.

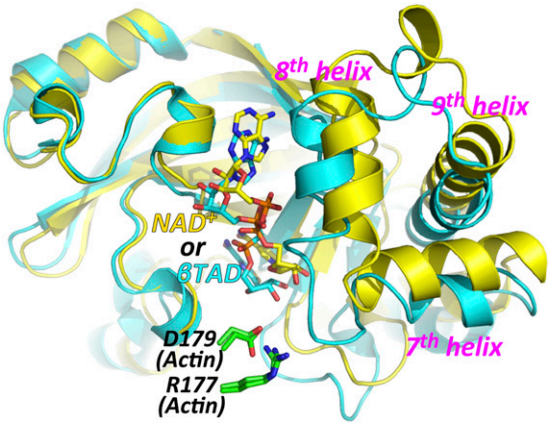

Fig. S4. Superposition of NAD^+-Ia-actin (Ia: yellow) and βTAD-Ia-actin (Ia: cyan). Actin and other cofactors are depicted in the same color as the previous figures (Fig. 1). Two structures show similar conformation, except the seventh, eighth, and ninth helices (labeled in magenta) in the C-terminal domain of Ia.

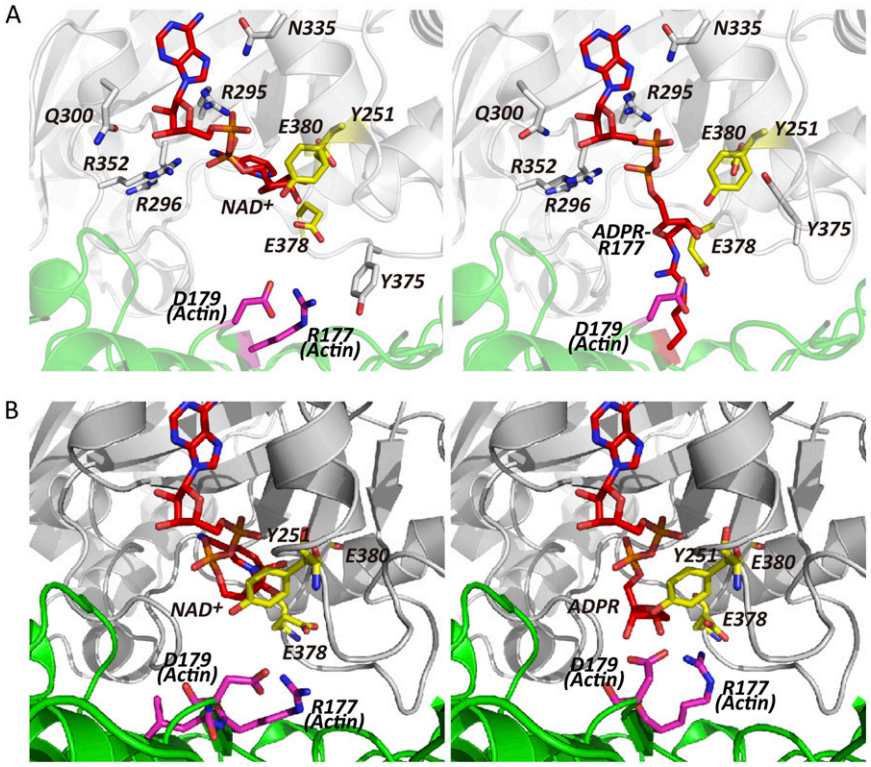

Fig. S5. Comparison between observed structure and old model. (*A*) Observed structures in NAD^+-Ia-actin (*Left*) and Ia-ADPR-actin (*Right*) in present study. (*B*) Old models in previous report (1): NAD^+ binding model (*Left*) and second intermediate model (*Right*). NAD^+ and ADPR-arginine are depicted in red, mobile residues in Ia are represented in yellow, and R177 and D179 of actin are in magenta.

Table S1. Data collection and structure refinement statistics of apo-Ia-actin, NAD^+-Ia-actin, and Ia-ADPR-actin

	apo-Ia-actin	NAD^+-Ia-actin	Ia-ADPR-actin
Unit cell (Å)	a = 53.9, b = 135.0, c = 154.5	a = 54.4, b = 135.9, c = 153.10	a = 54.0, b = 134.2, c = 151.0
Space group	$P2_12_12_1$	$P2_12_12_1$	$P2_12_12_1$
Beamline	PF-AR NW-12	PF BL-5A	PF BL-5A
Resolution (Å)	50.0–2.7	50.0–1.75	50.0–2.20
No. of reflections	31,910 (1,539)	110,554 (5,154)	56,709 (2,789)
Completeness	99.8 (99.5)	96.4 (90.9)	99.9 (99.6)
R_{sym}	0.076 (0.390)	0.040 (0.351)	0.040 (0.327)
I/σ	9.9	19.9	13.7
Redundancy	7.1	5.5	7.2
R_{work}/R_{free}	0.224/0.262	0.216/0.233	0.212/0.239
rmsd bond length/bond angle	0.008/1.332	0.006/1.420	0.006/1.472

Values in parentheses are for the last resolution shell. $R_{sym} = \sum h \sum i |Ii(h) - \langle I(h) \rangle| / \sum h \sum i |Ii(h)|$, where $Ii(h)$ is the intensity measurement for a reflection h, and $\langle I(h) \rangle$ is the mean intensity for this reflection. $R_{work} = \sum h ||F_{obs}| - |F_{calc}|| / \sum h |F_{obs}|$. R_{free} was calculated with randomly selected reflections (5%). All structures with no residue in the outlier region were analyzed with Ramachandran plot.

Table S2. Data collection and structure refinement statistics of NAD^+-Ia (mutants)-actin

	NAD^+-IaE378S-Actin	NAD^+-IaE380A-Actin	NAD^+-IaE380S-Actin
Unit cell (Å)	a = 53.9, b = 134.9, c = 153.9	a = 54.0, b = 134.2, c = 151.1	a = 53.9, b = 134.9, c = 154.3
Space group	$P2_12_12_1$	$P2_12_12_1$	$P2_12_12_1$
Beamline	PF BL-5A	PF BL-5A	PF BL-5A
Resolution (Å)	50.0–2.03	50.0–2.36	50.0–1.94
No. of reflections	71,718 (3,382)	47,500 (1,949)	83,852 (4,100)
Completeness	97.6 (92.3)	97.3 (92.0)	99.9 (99.5)
R_{sym}	0.038 (0.322)	0.051 (0.191)	0.063 (0.292)
I/σ	17.0	24.9	29.6
Redundancy	6.1	6.4	5.3
R_{work}/R_{free}	0.215/0.234	0.224/0.251	0.219/0.233
rmsd bond length/bond angle	0.006/1.438	0.007/1.343	0.006/1.624

Values in parentheses are for the last resolution shell. $R_{sym} = \sum h \sum i |Ii(h) - \langle I(h) \rangle| / \sum h \sum i |Ii(h)|$, where $Ii(h)$ is the intensity measurement for a reflection h, and $\langle I(h) \rangle$ is the mean intensity for this reflection. $R_{work} = \sum h ||F_{obs}| - |F_{calc}|| / \sum h |F_{obs}|$. R_{free} was calculated with randomly selected reflections (5%). All structures with no residue in the outlier region were analyzed with Ramachandran plot.

Table S3. Residue–residue interaction between Ia and actin (3.5-Å cutoff)

Ia-actin	Distance (Å)	Interaction
Y60-E276	2.61	Ionic bond
Y60-N280	3.24	Hydrogen bond
D61-K284	3.16	Ionic bond
Y62-N280	2.61	Hydrogen bond
Y311-E270	2.58	Ionic bond
S347-M176	3.35	Hydrogen bond
S347-S271	3.39	Hydrogen bond
S347-N280	2.84	Hydrogen bond
K351-E270	2.89	Ionic bond
K351-E276	2.78	Ionic bond
R352-E270	3.39	Ionic bond

Table S4. Properties of residues Glu378, Glu380, and Tyr375

Residue	Glu378	Glu380	Tyr375
Activities by mutational study*			
NADase	↓	↓↓↓	ND
ARTase	↓↓↓	↓↓↓	ND
Distance from $NAD^{+\dagger}$	++ (*N*-ribose)	++ (*N*-ribose)	–
Nicotinamide cleavage (I) or transferase (II)	I, II	I	II
Role and comment	It is a conserved and flexible residue on ARTT loop. After nicotinamide clevage, this residue may make *N*-ribose rotation. It may have recognized Arg177 of actin, but it was not trapped in our static structure.	It is a conserved and rigid residue on ARTT loop. This is essential for formation of NMN ring-like conformation.	It is conserved Tyr/Phe and flexible residue on ARTT loop. This residue seems to be important with substrate protein (actin) recognition.

Arrows indicate decreased degree of enzyme activity upon single mutaion to alanine; ↓↓↓ means almost diminished. ARTT, ADP-ribosylating turn-turn; ND, not determined. NMN, nicotinamide mononucleotide.

*"Mutational study" refers to Nagahama et al. (1) and our previous report (2).

†Distances cut off with "++" within 4 Å, "+" from 4 to 6 Å, and "–" over 6 Å.

1. Nagahama M, Sakaguchi Y, Kobayashi K, Ochi S, Sakurai J (2000) Characterization of the enzymatic component of Clostridium perfringens iota-toxin. *J Bacteriol* 182(8):2096–2103.
2. Tsuge H, et al. (2003) Crystal structure and site-directed mutagenesis of enzymatic components from Clostridium perfringens iota-toxin. *J Mol Biol* 325(3):471–483.

Table S5. Properties of residues Ser338 and Phe349

Residue	Ser338	Phe349
Activities by mutational study*		
ARTase	↓↓↓	↓↓↓(Ala), no decrease (Tyr)
NADase	↓↓↓	↓↓↓(Ala), ↓↓(Tyr)
Distance from NAD$^{+\dagger}$	+ (nicotinamide)	+ (nicotinamide)
Nicotinamide cleavage (I) or transferase (II)	I	I
Role and comment	These residues are STS motif, and Ser338 fixes nicotinamide as head part of scorpion structure.‡	This residue, as tip of scorpion tail, may fix nicotinamide.‡

Arrows indicate decreased degree of enzyme activity upon single mutaion to alanine; ↓↓↓ means almost diminished. ARTT, ADP-ribosylating turn-turn; ND, not determined. NMN, nicotinamide mononucleotide.
*"Mutational study" refers to Nagahama et al. (1) and our previous report (2).
†Distances cut off with "++" within 4 Å, "+" from 4 to 6 Å, and "−" over 6 Å.
‡This conformation is referred to in ref. 3.

1. Nagahama M, Sakaguchi Y, Kobayashi K, Ochi S, Sakurai J (2000) Characterization of the enzymatic component of Clostridium perfringens iota-toxin. *J Bacteriol* 182(8):2096–2103.
2. Tsuge H, et al. (2003) Crystal structure and site-directed mutagenesis of enzymatic components from Clostridium perfringens iota-toxin. *J Mol Biol* 325(3):471–483.
3. Lee YM, et al. (2010) Conserved structural motif for recognizing nicotinamide adenine dinucleotide in poly(ADP-ribose) polymerases and ADP-ribosylating toxins: Implications for structural-based drug design. *J Med Chem* 53:4038–4049.

Table S6. Properties of residues Tyr251, Arg295, and Arg296

Residue	Tyr251	Arg295	Arg296 (main chain)
Activities by mutational study*			
NADase	↓↓↓	ND	
ARTase	↓↓↓	ND	
Distance from NAD$^{+\dagger}$	++ (*N*-ribose)	++ (*N*-phosphate)	++ (nicotinamide)
Nicotinamide cleavage (I) or transferase (II)	I, II	I, II	I
Role and comment	This may be related to nicotinamide cleavage and transferace activity via making cation-π interaction with *N*-ribose.	ADP moiety gripping	ADP moiety gripping

Arrows indicate decreased degree of enzyme activity upon single mutaion to alanine; ↓↓↓ means almost diminished. ARTT, ADP-ribosylating turn-turn; ND, not determined. NMN, nicotinamide mononucleotide.
*"Mutational study" refers to Nagahama et al. (1) and our previous report (2).
†Distances cut off with "++" within 4 Å, "+" from 4 to 6 Å, and "−" over 6 Å.

1. Nagahama M, Sakaguchi Y, Kobayashi K, Ochi S, Sakurai J (2000) Characterization of the enzymatic component of Clostridium perfringens iota-toxin. *J Bacteriol* 182(8):2096–2103.
2. Tsuge H, et al. (2003) Crystal structure and site-directed mutagenesis of enzymatic components from Clostridium perfringens iota-toxin. *J Mol Biol* 325(3):471–483.

Table S7. Properties of residues Gln300, Asn335, and Arg352

Residue	Gln300	Asn335	Arg352
Activities by mutational study*			
NADase	ND	ND	↓↓↓
ARTase	ND	ND	↓↓↓
Distance from NAD+†	++ (A-ribose)	++ (adenine)	++ (A-phosphate)
Nicotinamide cleavage (I) or transferase (II)	I, II	I, II	I, II
Role and comment	ADP moiety gripping	ADP moiety gripping	ADP moiety gripping

Arrows indicate decreased degree of enzyme activity upon single mutaion to alanine; ↓↓↓ means almost diminished. ARTT, ADP-ribosylating turn-turn; ND, not determined. NMN, nicotinamide mononucleotide.
*"Mutational study" refers to Nagahama et al. (1) and our previous report (2).
†Distances cut off with "++" within 4 Å, "+" from 4 to 6 Å, and "−" over 6 Å.

1. Nagahama M, Sakaguchi Y, Kobayashi K, Ochi S, Sakurai J (2000) Characterization of the enzymatic component of Clostridium perfringens iota-toxin. *J Bacteriol* 182(8):2096–2103.
2. Tsuge H, et al. (2003) Crystal structure and site-directed mutagenesis of enzymatic components from Clostridium perfringens iota-toxin. *J Mol Biol* 325(3):471–483.